Research Article

Received: 30 September 2021 Revised: 27 December 2021 Accepted article published: 9 January 2022 Published online in Wiley Online Library: 23 January 2022

(wileyonlinelibrary.com) DOI 10.1002/pi.6364

Regulated acrylate networks as tough photocurable materials for additive manufacturing

Markus Kury,[a] Katharina Ehrmann,[a] Christian Gorsche,[a] Peter Dorfinger,[b] Thomas Koch,[b] Jürgen Stampfl[b] and Robert Liska[a*]

Abstract

In lithography-based additive manufacturing, mostly crosslinking monomers with acrylate functionality are applied, which yield brittle materials with inhomogeneous network architectures. The toughening of state-of-the-art materials is an integral requirement for the advancement of photopolymer-based three-dimensional (3D) products. Here we show that the final material properties of acrylate networks can be adjusted through regulation of the radical curing mechanism using difunctional vinyl sulfonate esters to obtain toughened 3D structured materials. A substantial improvement of the thermomechanical behavior of resulting materials over materials regulated by state-of-the-art reagents (e.g. thiols) is presented and first 3D parts have successfully been printed. Resulting materials exhibit reduced shrinkage stress, reduced warpage, higher overall conversion and higher glass transition temperatures compared with the pure acrylate network.

Supporting information may be found in the online version of this article.

Keywords: addition–fragmentation chain transfer (AFCT); photopolymerization; additive manufacturing; acrylate; thiol–ene; tough photopolymer

INTRODUCTION

Additive manufacturing technologies are currently blazing the trail to the future from creating non-functional, illustrative objects to providing customized functional parts, which are difficult to manufacture by conventional means. For this objective, the importance of material properties has increased tremendously in additive manufacturing and specifically for photolithographic methods.[1] While stereolithographic printing brings along important advantages for the manufacturing of functional parts (e.g. speed, resolution, surface quality), the photopolymeric materials that are available for this technology currently do not meet the high expectations regarding their thermomechanical performance in conjunction with improved toughness.[2]

Nowadays, acrylates represent by far the largest and most important group of radically cured monomers. The unregulated and fast free radical photopolymerization of multifunctional acrylate monomers leads to high crosslinking densities and gelation at low double bond conversion (DBC). This manifests in inhomogeneous, brittle networks, and high shrinkage stress in the material. The state-of-the-art method for regulating free radical photopolymerization of acrylates is thiol–ene chemistry.[3] Thiol–ene chemistry shows great performance in photopolymerization when it comes to reducing polymer shrinkage,[4] modifying glass transition temperature[5] and increasing toughness.[6] However, its application comes with drawbacks such as strong odor,[7] low storage stability[8] and the formation of flexible thioether bridges yielding soft material.[9] These disadvantages of thiol–ene chemistry stimulate the demand for alternative methods for modifying acrylate-based networks.

Irreversible addition–fragmentation chain transfer (AFCT) provides a solution to these problems, without AFCT reagents absorbing too much UV–visible light for photocuring or drastically decreasing polymerization speeds as would be the case for reversible addition–fragmentation chain transfer or atom transfer radical polymerization.[10–12] While thiol–acrylate chemistry turns a chain growth mechanism into a mixed chain growth/step growth mechanism (Fig. S7),[3,13,14] AFCT reagents use a slightly different approach to regulate free radical polymerization. Basically, an AFCT reagent consists of a reactive double bond, an activating group A, a cleavable group C (e.g. methylene or oxygen) and a leaving group L (Fig. 1 and Fig. S8). Group A defines the reactivity

* *Correspondence to: R Liska, Institute of Applied Synthetic Chemistry, Technische Universität Wien, Getreidemarkt 9/163 MC, 1060 Vienna, Austria, E-mail: robert.liska@tuwien.ac.at*

a *Institute of Applied Synthetic Chemistry, Technische Universität Wien, Vienna, Austria*

b *Institute of Materials Science and Technology, Technische Universität Wien, Vienna, Austria*

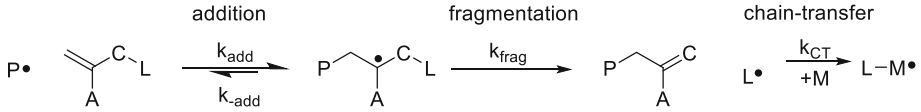

Figure 1. Structure and mechanism of a generic AFCT reagent.

of the double bond of the AFCT reagent, while L should be a molecule that forms a reinitiating radical. When the radical of a growing polymer chain (P) attacks the unsaturated carbon–carbon bond of the AFCT reagent and undergoes an addition reaction, an intermediate radical is formed. This can, on the one hand, perform a back reaction to regenerate the starting species or, on the other hand, fragment via β-scission to give a reactive leaving group radical, which in turn reinitiates a new chain.[15]

Like thiols, AFCT reagents may shorten the kinetic chain length of the growing polymer backbones. In multifunctional systems, this ability of regulating free radical polymerization can be used to tune network properties, reduce crosslinking density and delay the gel point to higher DBCs. This shift of gelation allows a resin to remain in liquid aggregate up to higher DBC and built up mechanical stress can dissipate in the resin, which results in significantly reduced shrinkage stress,[16] sharper glass transitions and higher toughness.[17–19]

While this approach has already been tested successfully for methacrylate monomers,[15,20] the high reaction rate of acrylates may challenge its effectivity for this monomer class. Therefore, we present a detailed analysis of the modification ability of a difunctional vinyl sulfonate ester in a difunctional acrylate matrix. As a contrast, a difunctional thiol of similar structure is used to directly compare the performance of the vinyl sulfonate ester with the state-of-the-art method. Therefore, a variety of experiments are described including photorheology, dynamic mechanical thermal analysis (DMTA), tensile testing, Dynstat impact resistance and nanoindentation. Finally, three-dimensional (3D) parts are printed using a DLP printer to showcase the potential for 3D printing.

EXPERIMENTAL

Materials

1,6-Hexanediol diacrylate (HDDA) was purchased from Alfa Aesar as monomer matrix. Ivocerin® was kindly provided by Ivoclar Vivadent. The dithiol tetraethylene glycol bis(3-mercaptopropionate) (DT) was purchased from Wako. ((Oxybis(ethane-2,1-diyl))bis (oxy))bis(ethane-2,1-diyl) bis(2-(tosyloxy)acrylate) (DVS) was used as an AFCT reagent and was synthesized as described previously.[20]

Formulations and specimens

HDDA was chosen as matrix and germanium-based Ivocerin® as photoinitiator[21] for the mechanical study. For guaranteeing network regulation, DVS was applied as AFCT network modifier and the dithiol DT was used in thiol–ene regulated networks.

Neat HDDA, DT and DVS mixtures were prepared according to Table 1. To all formulations 0.3 wt% of photoinitiator Ivocerin® was added and the substances were homogenized by vortexing and in an ultrasonic bath at 40 °C for at least 30 min. The prepared formulations were directly used for real-time near-infrared (RT-NIR) photorheology and storage stability measurements. For mechanical tests, test specimens were cured in silicon molds in a Lumamat 100 light oven provided by Ivoclar Vivadent AG. The light oven was equipped with 6 Osram Dulux L Blue lamps (18 W, 400–580 nm). The light intensity of *ca* 20 mW cm^{-2} was determined with an Ocean Optics USB 2000+ spectrometer at the position of the silicone molds. The total curing time was 600 s, whereby the specimens were turned after 300 s and the backside was irradiated for another 300 s. Finally, the cured specimens were sanded and polished to comply with the required specifications.

RT-NIR photorheology

The RT-NIR photorheometer consisted of an Anton Paar MCR 302 WESP with a P-PTD 200/GL Peltier glass plate and a disposable PP25 measuring system coupled with a Bruker Vertex 80 FTIR spectrometer.[22] For measuring IR spectra, external mirrors guided the IR beam from the spectrometer through the flat glass plate and the sample to the flat rheology plate, where the beam was reflected and led to an external MCT detector. For every monomer formulation, 130 µL was placed on the glass plate. The measuring temperature was 20 °C and the gap between the glass plate and a stainless steel PP25 plate was 200 µm. The measurements were conducted in oscillation mode with a strain of 1% and a frequency of 1 Hz. For irradiating the samples, an Exfo OmniCure™ 2000 with a broad-band Hg lamp was used. The light with a wavelength between 400 and 500 nm was led through a dual leg light guide, of which the tips were located directly under the glass plate. The irradiation intensity was 10 mW cm^{-2} at the surface of the sample. Every formulation was measured at least three times. During the measurement, the storage modulus (G'), loss modulus (G'') and normal force (F_N) were recorded. At the beginning of the measurement (first 60 s), one measurement point per second was recorded without irradiating the sample. Afterwards, the sample was irradiated for 5 min in total. During the first minute of irradiation, 0.2 measurement points per second were recorded and during the last 4 min, the sampling rate was again reduced to one measurement point per second. In order to monitor the DBC, RT-NIR analysis was conducted *in situ*. Therefore, a single spectrum was recorded every *ca* 0.2 s. An OPUS 7.0 software tool was used to process the spectra and to integrate the relevant DB bands at *ca* 6160 cm^{-1}. At this point it must be emphasized that the DBC of DT formulations does not include the unreacted thiol groups, but only the HDDA signals. In the case of DVS formulations, the DBC signal comprises the HDDA and the DVS signals. Important key parameters that can be extracted from the recorded mechanical and chemical data are the time until gelation point (t_{gp}), the DBC at gel point (DBC_{gp}), the final DBC after irradiation is finished (DBC_{final}), the time after 95% of the final DBC is reached as a measure for reaction speed and completeness, the final storage modulus (G'_{end}) as well as the normal force (F_N) as a measure for the evaluation of shrinkage stress. The gel point was determined as the first intersection of G' and G'' after the start of irradiation. The frequency-dependent gel point was only determined at one frequency and can therefore only be seen as relative value for comparing the gelation speed of the tested samples. The photorheology setup and additional information can be found in the supporting information (Appendix S1).

Polymer International published by John Wiley & Sons Ltd on behalf of Society of Industrial Chemistry.

Table 1. Composition of formulations containing pure HDDA or mixtures of HDDA with either DT or DVS as regulator (5, 10, 20 or 35 mol%)

Formulation	HDDA (mol%)	DT (mol%)	DVS (mol%)
HDDA	100	—	—
DT5	95	5	—
DT10	90	10	—
DT20	80	20	—
DT35	65	35	—
DVS5	95	—	5
DVS10	90	—	10
DVS20	80	—	20
DVS35	65	—	35

Dynamic mechanical thermal analysis

Rectangular specimens (*ca* $5 \times 2 \times 40$ mm^3) were cured and polished to obtain exact geometries for the specimens. DMTA measurements were performed using an Anton Paar MCR 301 with a CTD 450 oven and an SRF 12 measuring system. The temperature range was set from −100 to 200 °C with a heating rate of 2 °C min^{-1}. The prepared polymer specimens were tested in torsion mode with a frequency of 1 Hz and 0.1% strain. Rheoplus/32V3.40 from Anton Paar was used as software tool to evaluate and process the recorded data. The crosslinking density (ρ) was calculated from the storage modulus in the rubbery state (G'_{rubber}) as described in the literature[23,24] (see Appendix S1 in the supporting information).

Tensile tests

Dog bone-shaped tensile test specimens were prepared according to ISO 527 test specimen 5b. The tensile tests were performed using a Zwick Z050 equipped with a 1 kN load cell at room temperature. The specimens were fixed between two clamps and strained with a traverse speed of 5 mm min^{-1}. The measurements were performed without using an extensometer.

Dynstat impact resistance

Rectangular specimens (*ca* $10 \times 2 \times 15$ mm^3) were cured. The Dynstat tests were carried out with a 1 J hammer. Sample DVS35 was measured with a 2 J hammer because of the significantly higher impact resistance of the material. Experiments were conducted in quadruplicate. It was not possible to obtain results for the DT20 and DT35 samples, because even the 2 J hammer was not able to break the specimens, since they were too soft.

Nanoindentation

Nanoindentation experiments were carried out with a Hysitron TI 750L Ubi. The remainders of the Dynstat impact resistance polymer specimens were indented with a loading rate of 0.1 mN s^{-1} and then held at the maximum load of 1 mN for 30 s. Finally, the load was released with an unloading rate of 0.2 mN s^{-1}. Five repetitions were performed for each composition.

Storage stability

The prepared monomer formulations were analyzed with a modular compact rheometer (MCR 300 Physica, Anton Paar). The viscosity measurements were carried out at 20 °C with a CP-25 measuring system (diameter 25 mm). The distance between tip and plate was set to 48 µm and a shear rate of 100 s^{-1} was applied. The overall measuring time was set to be 100 s and every 5 s a measuring point was recorded. The collected data were analyzed using Rheoplus/32V3.40 software from Anton Paar. Subsequently, the formulations were stored in the dark in an amber 20 mL vial at 37 °C for 120 days. The formulations were checked for premature gelation at regular intervals (first 3 weeks almost daily, after that twice a week). After storage, viscosity was measured once again as described above and compared with the initial results. Samples DT10, DT20 and DT35 had already gelled after 120 days of storage and therefore rheology measurements could not be conducted for these samples.

Digital light processing

The 3D structuring of HDDA containing 10 mol% DVS (DVS10) was performed with a lithographic bottom-up DLP printer prototype that was equipped with a light source with a maximum emission at 460 nm. The light intensity on the surface of the material vat was measured to be 30 mW cm^{-2}. In order to obtain high resolution for the printed parts, an additional 0.1 wt% of Sudan yellow was mixed into the DVS10 formulation as absorber. The exposure time was set to 10 s to obtain an adjusted layer thickness of 50 µm for each layer. The final printed 3D parts were cleaned from any residual resin with compressed air and sonicated in isopropanol for 1 min before being dried at ambient conditions overnight. A post-processing step in an IntelliRay 600UV oven with a broadband Hg lamp was conducted afterwards to finalize the radical polymerization (300 s, 600 W, *ca* 280–550 nm, UV-A: 125 W cm^{-2}, visible: 125 mW cm^{-2}, total irradiation intensity of 200 mW cm^{-2} at the position of the samples).

Scanning electron microscopy

The SEM images of the 3D-printed parts were obtained with an XL-30 microscope (Philips). The printed structure was sputtered with a conducting gold layer and images were recoded with varying magnification.

Swelling tests

Polymer platelets with a diameter of 2 mm and a height of 1 mm were cured. These platelets were weighed (m_{start}) and subsequently submerged in ethanol containing 200 ppm hydroquinone monomethyl ether for 14 days at 25 °C. The ethanol solution was changed after 1, 5, 8 and 11 days. After 14 days, the polymer disc surfaces were dried with a paper towel to remove excessive ethanol and weighed ($m_{swollen}$). Finally, the polymer pellets were dried in a 60 °C vacuum oven until constant weight was reached (m_{dry}). Experiments were conducted in triplicate for each composition. The results can be found in the supporting information (Appendix S1).

RESULTS AND DISCUSSION

Formulations and materials

In order to carry out a comparative study for the applicability of vinyl sulfonate esters for regulating acrylate networks, a previously established AFCT reagent, the difunctional vinyl sulfonate ester DVS, was applied in curing experiments of the model acrylate HDDA. For comparison, the dithiol DT was selected as chain transfer agent (CTA) acting in a thiol–ene regulating manner (Fig. 2).

For this purpose, 5, 10, 20 and 35 mol% of the thiol- and vinyl sulfonate ester-based CTAs were mixed with HDDA and 0.3 wt%

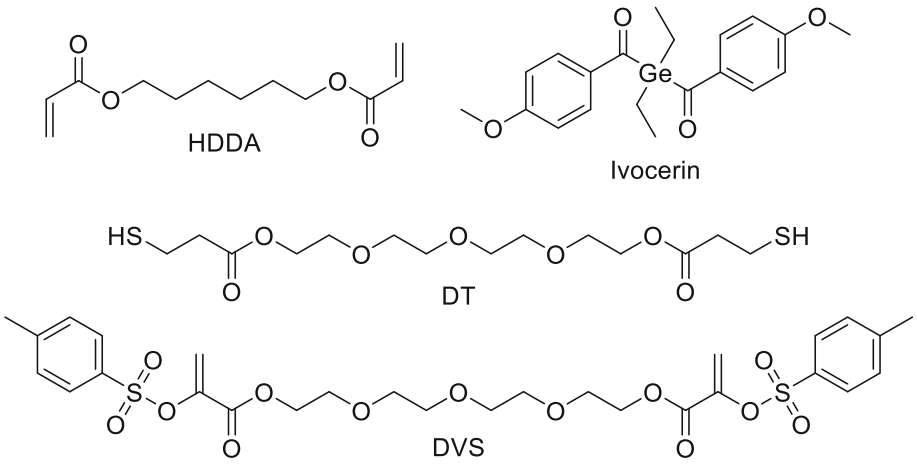

Figure 2. Structures of monomer HDDA, photoinitiator Ivocerin® as well as DT and DVS as CTAs.

of photoinitiator Ivocerin® was added additionally to the formulations (Table 1).

The formulations were directly used for the photoreactivity and storage stability tests, while the specimens for mechanical tests were polymerized in silicone molds in a UV–visible light furnace.

Formulation tests

RT-NIR photorheology

To determine the influence of both DVS and DT on the acrylate formulation, RT-NIR photorheology was conducted, a powerful tool for simultaneously recording fluid mechanical data of the formulations, mechanical data and DBC of the cured solid photopolymer, and the transition between these two aggregate states (Fig. S1).

In vat polymerization-based additive manufacturing techniques, gelation time, i.e. the transition of a liquid photoresin to a solid photopolymer, is of particular importance for the printing speed. The time until the gel point is reached (t_{gp}) can be deferred from the recorded moduli, whereby the gel point in this work is defined as the intersection between storage modulus (G') and loss modulus (G'') at a frequency of 1 Hz. As is evident from Table 2, the gel point of the neat acrylate formulation is reached fastest of all tested formulations after only 1.0 s, as expected. The DBC, inferred from the *in situ* IR signals during curing, is very low at the gel point (8%). This confirms the early transition from liquid to solid at low conversions. Nevertheless, the final DBC reaches a rather high level (89%) and the reaction takes 30 s until the final DBC is reached (t_{95}). This reflects that the radical crosslinking reaction occurs predominantly in the solid state, which is mirrored in the high normal force (F_N) value (46 N). In the presented experiments, the F_N value is the force necessary to maintain the gap between rheometer stamp and plate at the initially set distance of 200 µm when polymerization-induced shrinkage occurs. Hence, F_N can be seen as a measure for the evaluation of shrinkage stress. These parameters already reflect that regulation of this system is more challenging than for methacrylates.[20]

As expected, the addition of thiols delays the gel point slightly (1.6–2.7 s). However, the delay comes with higher DBC_{gp} increasing with thiol concentration from 18% for DT5 up to 55% for DT35. With higher DBC_{gp}, fewer double bonds are left in the solid state to react, leading to a decrease in F_N that is particularly pronounced at higher thiol concentrations (e.g. 33 N for DT20 or 25 N for DT35). Simultaneously, DBC_{final} reaches over 90% of full conversion (Fig. 3 and Fig. S3) and t_{95} significantly decreases, indicating a faster completion of the reaction, while the modulus decreases with increasing DT content. Similar findings can be reported for the DVS formulation. Here, the t_{gp} delay is already significantly higher for DVS5 (3.8 s) and increases to 7.3 s for DVS35. Nevertheless, DBC_{gp} is rather high when compared to those of thiols starting at 31% for DVS5 and finishing at 70% for DVS35. The emerging normal force is therefore correspondingly low at 41 N for DVS5 and only 18 N for DVS35 (Fig. S4). The values of t_{95} are also reduced with increasing DVS content, and so are the final storage moduli (Fig. S2).

Comparing the vinyl sulfonate ester with thiol regulation (Fig. 3 and Fig. S2-S4) clearly indicates that the reaction rate of thiols is high and in the range of homopolymerization, while vinyl sulfonate esters show a slight delay. It is assumed that the retardation in DVS formulations arises from the more complex scission mechanism of AFCT reagents in contrast to thiols. Nevertheless, DBC_{gp} is in all cases higher for DVS-modified formulations than for DT formulations. This is particularly pronounced when low CTA concentrations are considered (e.g. DT5 *versus* DVS5). An explanation for this might be the longer t_{gp} of DVS-regulated formulations giving the resin more time to reach higher DBC before solidification. The same assumption would account for the smaller detected F_N values for cured DVS formulations. However, both CTAs are highly suitable for adaptation of fast-curing acrylate systems keeping the reaction speed high and reducing the formation of material shrinkage stress.

Storage stability of formulations

Poor storage stability for non-stabilized thiol–acrylate formulations even at low temperatures is a well-known issue in the photopolymer community. Therefore, vinyl sulfonate esters as CTAs could be welcome substitutes with superior stability. Initial viscosities of CTA-containing formulations increased with increasing CTA contents for both additives, with that of DVS being more pronounced (Table 2). Upon storage, the pure HDDA formulation as well as the DVS-containing mixtures remained liquid for the predetermined storage period of 120 days. Addition of DVS only led to a slight increase of viscosity at 35 mol% that is not expected to significantly affect the resin processibility. The addition of DT, however, led to premature gelation before 120 days had passed already at low concentrations from 10 mol% on. For higher concentrations, the solidification was only a matter of days. The

Table 2. Results of RT-NIR photorheology study for pure HDDA and its mixtures with 5, 10, 20 or 35 mol% either DT or DVS: time until gelation (t_{gp}), DBC at the gel point (DBC_{gp}), time until 95% conversion (t_{95}), storage modulus at final conversion (G'_{end}) and normal force at final conversion (F_N), as well as storage stability results determined via rheology measurement

	RT-NIR photorheology						Storage stability	
Formulation	t_{gp} (s)	DBC_{gp} (%)	t_{95} (s)	DBC_{final} (%)	G'_{end} (MPa)	F_N (N)	η (0 days) (mPa s)	η (120 days) (mPa s)
HDDA	1.0 ± 0.1	8 ± 1	30 ± 1	89 ± 1	0.96 ± 0.02	46 ± 1	8	8
DT5	1.6 ± 0.1	18 ± 1	22 ± 1	92 ± 1	0.90 ± 0.01	45 ± 1	9	9
DT10	2.2 ± 0.1	33 ± 1	12 ± 1	96 ± 1	0.88 ± 0.01	40 ± 1	10	gel (5 days)
DT20	1.7 ± 0.1	38 ± 1	7 ± 1	100 ± 0	0.70 ± 0.01	33 ± 1	13	gel (10 days)
DT35	2.7 ± 0.1	55 ± 2	6 ± 1	100 ± 0	0.58 ± 0.04	25 ± 1	33	gel (*ca* 80 days)
DVS5	3.8 ± 0.1	31 ± 1	26 ± 1	91 ± 1	0.96 ± 0.02	41 ± 1	11	11
DVS10	4.8 ± 0.1	37 ± 1	20 ± 1	93 ± 1	0.89 ± 0.01	36 ± 1	17	17
DVS20	5.8 ± 0.1	47 ± 2	19 ± 1	97 ± 1	0.81 ± 0.01	25 ± 1	35	37
DVS35	7.3 ± 0.2	70 ± 2	18 ± 1	100 ± 0	0.77 ± 0.03	18 ± 1	102	114

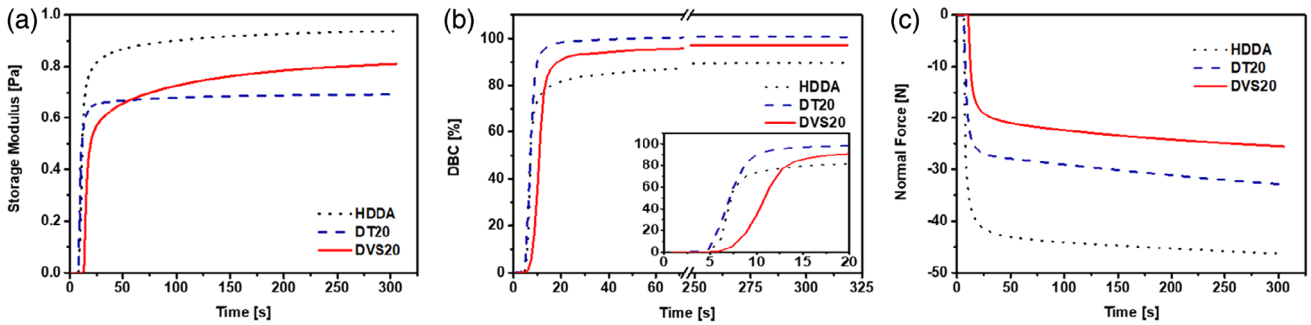

Figure 3. Comparison of photocuring behavior of pure HDDA and its mixtures with 20 mol% DT (DT20) and DVS (DVS20): development of (a) G', (b) DBC and (c) F_N with curing time during photorheology.

suspected poor storage stability of thiol-containing formulations and the excellent stability of vinyl sulfonate ester resins could therefore be confirmed.

Mechanical tests

Dynamic mechanical thermal analysis

To observe network regulation effects more closely, the thermomechanical properties of the produced CTA-modified photopolymers are particularly of interest. Therefore, a variety of key parameters were extracted from the DMTA data such as the storage modulus at 20 °C as application temperature and at the rubber plateau (G'_{20} and G'_{rubber}, respectively), the glass transition temperature (T_g), defined as maximum of the tan δ curve, and the full width at half maximum (FWHM) of the tan δ curve as a measure for the broadness of the glass transition. G'_{rubber} was also used to determine the crosslinking density (ρ; supporting information). While the results are presented for all concentrations of CTAs in Table 3, Fig. 4 only shows representative storage modulus and loss factor curves for formulations containing 20 mol% CTA. All other curves are shown in Fig. S5.

Neat unregulated HDDA matrix exhibits an E'_{20} around 1 GPa reaching T_g at 118 °C. A rubber modulus G'_{rubber} of 164 MPa hints at a high crosslinking density. The FWHM of the tan δ curve shows a broad range of 63 °C starting from 72 °C. With ρ of 46.9 mol L^{-1} the neat matrix also possesses the most crosslinks per volume. These values are typical for an inhomogeneous and glassy photopolymer with a broad glass transition region as is expected for an acrylate polymer.

Adding thiols to the formulation clearly influences the thermomechanical properties of the photopolymerized material. T_g, G'_{rubber} and ρ of the DT-derived polymers decrease significantly with increasing DT content compared to the neat matrix. Already small amounts of thiols result in significant declines of T_g (DT5 and DT10, 85 and 65 °C, respectively). Larger DT contents in the material even lead to T_g below 0 °C (DT20 and DT35). Substantial decreases can also be reported for G'_{rubber} and ρ, where the addition of 5 mol% dithiol almost cuts these values in half (84 MPa, 26.0 mol L^{-1}) compared to the unmodified photopolymer (164 MPa and 46.9 mol L^{-1}). Increasing the thiol content in the photocured thermosets even amplifies this effect (e.g. DT20 with G'_{rubber} of 17 MPa and ρ of 7.6 mol L^{-1}). While G'_{20} also declines with increasing DT content for most of the samples, DT10 represents an exception. Surprisingly, DT10 ends up at a slightly higher G'_{20} (770 MPa) than DT5 (760 MPa). This inconsistency will be discussed later in the nanoindentation section, since additional modulus data are presented there.

Explanations for the overall decrease of T_g and G'_{20} could be the formation of flexible thio–ether bridges that soften the final polymer and the reduced number of crosslinks in the material. As expected, the FWHM of the tan δ peaks tends to narrow with increasing DT content, which indicates a homogenization of the formed network architecture.

While expectedly similar trends in thermomechanical behavior hold true for the vinyl sulfonate ester-based specimens, their absolute values reflect superior performance of DVS over DT for several properties. Foremost, their superior behavior is

Table 3. Overview of key parameters determined using DMTA and tensile testing

	DMTA					Tensile testing	
Polymer	G'_{20} (MPa)	T_g (°C)	G'_{rubber} (MPa)	FWHM (°C)	ρ (mol L^{-1})	σ_{max} (MPa)	ε_B (%)
HDDA	980	118	164	63	46.9	38.7 ± 2.0	7.3 ± 1.4
DT5	760	85	84	50	26.0	29.5 ± 0.6	6.8 ± 0.6
DT10	770	65	52	40	17.0	21.9 ± 1.5	12.1 ± 2.8
DT20	20	−3	17	19	7.6	2.6 ± 0.7	15.2 ± 4.3
DT35	5	−34	5	11	2.2	1.2 ± 0.3	18.6 ± 6.8
DVS5	1110	92	90	45	27.4	43.5 ± 2.9	7.3 ± 2.0
DVS10	1150	71	45	29	14.5	48.9 ± 3.5	6.2 ± 1.0
DVS20	1465	48	18	17	5.8	51.0 ± 0.7	8.4 ± 0.7
DVS35	645	31	5	15	1.8	15.1 ± 3.1	113.7 ± 12.7

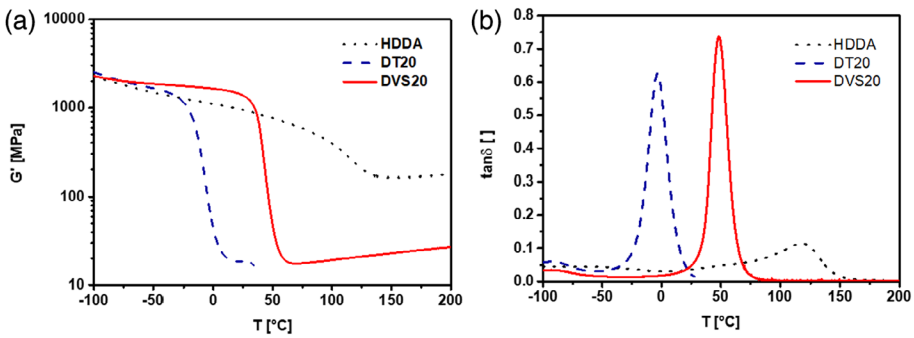

Figure 4. DMTA curves of (a) G' as a function of temperature and (b) tan δ as a function of temperature of HDDA, DT20 and DVS20.

demonstrated by a higher T_g at equal CTA concentrations and crosslinking densities, whereby this effect is particularly striking for CTA amounts of 20 and 35 mol%, where the difference in T_g exceeds 50 °C in both cases. Interestingly, the G'_{20} values for DVS-derived photopolymers also increase up to 20 mol% DVS content from 1110 to 1465 MPa. This behavior is impressive, since it illustrates a reverse trend compared to the DT-derived thermosets. However, G'_{20} of DVS35 decreases again (645 MPa) because the measuring temperature is close to its T_g.

Considering G'_{rubber} and ρ, DT- and DVS-based polymers exhibit values in the same range for all concentrations and generally following the trends described above for DT. The same is true for the decrease of FWHM of the tan δ peak, which indicates increasing network homogeneity with increasing regulation in both cases.

A good example is depicted in Fig. 4, where HDDA exhibits a wide glass transition region showing a steady decline of the G' curve and a broad tan δ curve with a low peak. On the other hand, the CTA-modified polymers display G' curves exhibiting a glassy region that is followed by a narrow and abrupt glass transition region showing a steep dive before reaching the rubbery plateau. In the case of tan δ, the peak of the CTA-derived material becomes considerably more pronounced and higher. However, T_g decreases compared to the acrylate homopolymer.

In summary, thiols and vinyl sulfonate esters represent important tools to modify acrylate photopolymers. Comparable crosslinking densities are achieved for equivalent amounts of CTA and more homogeneous network architectures are evident in both cases. In terms of T_g, the addition of vinyl sulfonate esters keeps T_g at higher values while T_g of thiol-containing polymers decreases significantly more.

Tensile tests

To assess the influence of the CTAs on the stress–strain behavior, tensile tests were conducted and the ultimate strength (σ_{max}) and the elongation at break (ε_B) were determined (Table 3; Fig. 5; Fig. S6).

The unregulated specimens of HDDA show curve shapes typical for thermosets with a tensile strength around 40 MPa and a low elongation at break ranging from 6% to 7%. Adding DT to the acrylate formulation leads to decreasing σ_{max} with increasing DT content, and for dithiol contents of 10 mol% or greater the elongation at break increases as well. Especially for DT20 and DT35, σ_{max} drops below 3 MPa, which can be linked to fact that both materials were tested in their rubbery state at room temperature.

In contrast to this, DVS contents up to 20 mol% even boost tensile strengths up to *ca* 50 MPa for 20 mol% (Fig. 5). This tendency follows the increasing G'_{20} measured using DMTA discussed in the previous subsection. Notably, the strain at break nonetheless remains in the range of HDDA between 6% and 8% at the same time. The only formulation falling out of this trend is DVS35, for which the tensile strength at break only reaches *ca* 15 MPa and exhibits *ca* 110% elongation at break (Fig. S6). This almost elastomer-like behavior can be explained by the fact that the testing temperature was close to the glass transition temperature of DVS35 and rubber-like behavior seems to dominate already.

Dynstat impact resistance

Highly brittle behavior and low impact resistance are critical drawbacks of photopolymers as well as of other typical thermosets. Therefore, we investigated if the improved mechanical behavior during tensile testing also translated into improved impact

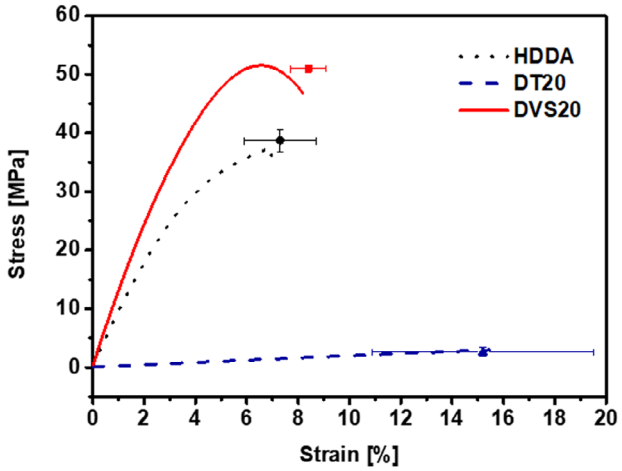

Figure 5. Tensile testing curves for pure HDDA and its mixtures DT20 and DVS20 and respective mean values for stress and strain at break.

resistance. For this purpose, Dynstat impact resistance tests were carried out for the photocured polymers.

As presented in Table 4, neat HDDA shows the most brittle behavior with an impact strength of about 5.5 kJ m^{-2}. DT-regulated specimens DT5 and DT10 already show an increase in impact resistance to 7.5 and 11.7 kJ m^{-2}. These findings are no surprise, since the addition of thiols results in less crosslinked materials, which are able to absorb more impact energy before breaking. For DT20 and DT35, their rubbery network state at testing temperature comes fully into play. Their low stiffness led to rubber-like deformation of the specimens so that the hammer could not break the samples. Upon impact, they simply jumped out of the sample holder undamaged.

DVS-enhanced samples also led to an increase in impact resistance with increasing DVS content even though the modulus at room temperature remained in the range of that of the neat matrix (Table 4). At 5 mol% of DVS, the impact resistance was doubled compared to the neat matrix (11 kJ m^{-2}). DVS10, DVS20 and DVS35 even showed a threefold, fourfold and eightfold increase, respectively. This enhanced toughness can be attributed to the decreasing number of crosslinks in the DVS-modified polymer network architecture. For fair comparison, it must be mentioned that the DVS35 material at room temperature was already close to its T_g, which explains the high impact strength of *ca* 40 kJ m^{-2}.

However, none of the fracture sites of the tested samples, including those of DVS35, exhibited any visible stress whitening or crazing and can therefore be considered typical brittle fractures. All in all, it can be concluded that the addition of CTAs leads to a reduction of crosslinks in the materials that display enhanced toughness if compared to the neat matrix. Comparison of the mean values of impact resistance between DVS and DT samples only makes sense if both materials are still in the glassy state. Therefore, only polymers containing 5 and 10 wt% CTA were compared. In those cases, impact resistance for DVS samples is slightly higher than for DT samples.

Nanoindentation

Due to reduced network densities in regulated networks, softening of the materials is expected. To evaluate the extent of softening, nanoindentation was carried out. From the recorded data, values for indentation hardness (H_i) and reduced modulus (E_r) could be extracted (Table 4).

Unregulated HDDA exhibited a hardness around 90 MPa and a reduced modulus of *ca* 1600 MPa. Dithiols in the final polymer led to an instant decrease in H_i and E_r. This decrease became greater with increasing thiol content. While the decrease in H_i and E_r for DT5 is still small, resulting in values *ca* 77 and 1570 MPa, respectively, hardness of DT10 is half that of HDDA and drops even more dramatically for higher dithiol along with E_r. The decreasing E_r from DT5 to DT10 is interesting, since it does not mirror the G'_{20} values collected during the DMTA measurement, where G'_{20} of both polymers are in the region of *ca* 760 MPa. Reflecting the overall trends, E_r value obtained from nanoindentation for DT10 seems more reasonable.

On the other hand, adding DVS up to 10 mol% even increases H_i and E_r of the material when compared to HDDA. This development matches well with the measured G'_{20} values from DMTA. DVS20 leads to a slightly decreased hardness of *ca* 70 MPa again that is even lower than that of the homopolymer, while E_r remains comparably high (*ca* 2100 MPa). An assumption for the increased G'_{20} from DMTA as well as E_r values could be the formation of more rigid crosslinks resulting from the DVS regulation mechanism.

However, at 35 mol% DVS content, the material is according to nanoindentation results in the rubbery state that leads to a collapse of H_i and E_r. This finding does not fully comply with the G'_{20} DMTA result (645 MPa). The reason for that can be found in the slightly higher measuring temperature for nanoindentation at 23 °C that led to a quick decrease of G' at 23 °C to *ca* 200 MPa.

Table 4. Overview of results for Dynstat, nanoindentation (indentation hardness H_i, reduced modulus E_r) and swelling (swellability S, gel fraction G) experiments for pure HDDA and its mixtures with 5–20 mol% DT or DVS CTAs

Polymer	Dynstat	Nanoindentation		Swellability	
	Impact strength (kJ m^{-2})	H_i (MPa)	E_r (MPa)	S (wt%)	G (wt%)
HDDA	5.5 ± 0.7	88.8 ± 9.9	1628 ± 173	3.3 ± 0.1	99.8 ± 0.2
DT5	7.5 ± 1.2	76.7 ± 16.5	1566 ± 216	5.2 ± 0.7	99.8 ± 0.2
DT10	11.7 ± 2.9	42.2 ± 7.7	975 ± 129	6.7 ± 0.3	99.5 ± 0.3
DT20	—	6.8 ± 0.4	37 ± 1	9.8 ± 0.3	99.1 ± 0.1
DT35	—	2.3 ± 0.2	13 ± 1	14.5 ± 0.1	95.7 ± 0.2
DVS5	10.8 ± 1.6	91.8 ± 6.5	1939 ± 95	2.5 ± 0.2	99.5 ± 0.2
DVS10	14.6 ± 2.5	129.0 ± 21.0	2641 ± 236	3.2 ± 0.4	99.3 ± 0.2
DVS20	20.0 ± 2.5	70.7 ± 9.9	2082 ± 224	8.2 ± 0.8	99.2 ± 0.2
DVS35	40.2 ± 5.6	1.8 ± 0.1	38 ± 3	15.3 ± 0.3	96.3 ± 0.1

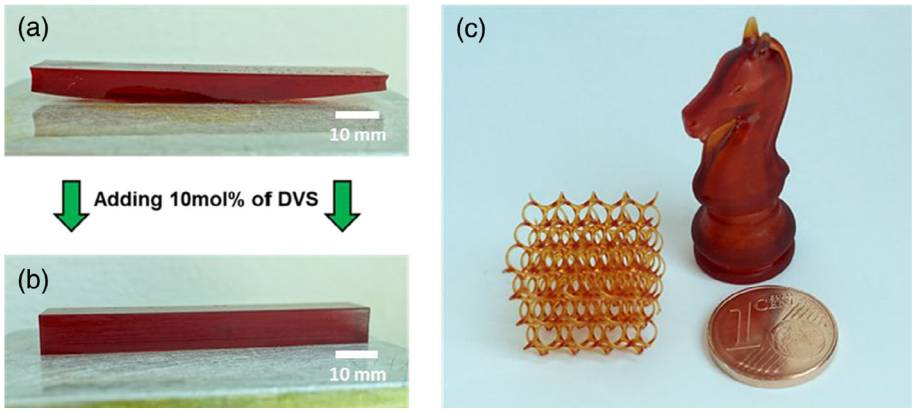

Figure 6. Printed block of (a) pure HDDA and (b) HDDA containing 10 mol% DVS. (c) More complex structures printed with DVS10.

Even though the measured E_r of 38 MPa is lower, this deviation can be attributed to the different measuring methods.

Summarizing, it can be stated that DT in the final polymer decreases the hardness of the samples with increasing DT amount. This finding is not surprising, since thiols are known to form flexible thio–ether bridges that soften the material. For DVS the hardness seems to remain unaffected for low concentrations (5 mol%), leads to harder material for medium concentrations (10 mol%) and softens the material again for higher concentrations (20 and 35 mol%).

Additive manufacturing

Digital light processing and SEM

Initial printing experiments were performed with a 460 nm DLP prototype printer operating in a bottom-up approach to show the potential of vinyl sulfonate esters for application in vat polymerization.

In a first experiment, a bulk rectangular block (80 × 20 × 10 mm^3) was printed from neat HDDA with 50 µm layer height. As can be seen in Fig. 6, the resulting specimen exhibits delamination from the building platform on both sides of the long edge of the rectangular specimen. This phenomenon can be attributed to the high internal shrinkage that detaches parts of the structure from the building platform leading to very great warpage.

To highlight the benefits of AFCT-regulated networks in 3D printing in contrast to neat acrylates, DVS was added to HDDA in a second experiment. A formulation with 10 mol% DVS (DVS10) was chosen to yield a photopolymer with a similarly high T_g for better comparison with neat HDDA. DVS10 was processed into the same rectangular block. The resulting printed part now exactly matches the geometry that was beforehand supplied to the printer software with no signs of delamination (Fig. 6). This can be explained by the higher DBC at the gel point, which leads to reduced stress in the material. Here it must be mentioned that this shift of the gel point to higher DBC usually comes with longer irradiation times to cure the resin into form-stable parts, which results in longer printing times. However, in the case of vinyl

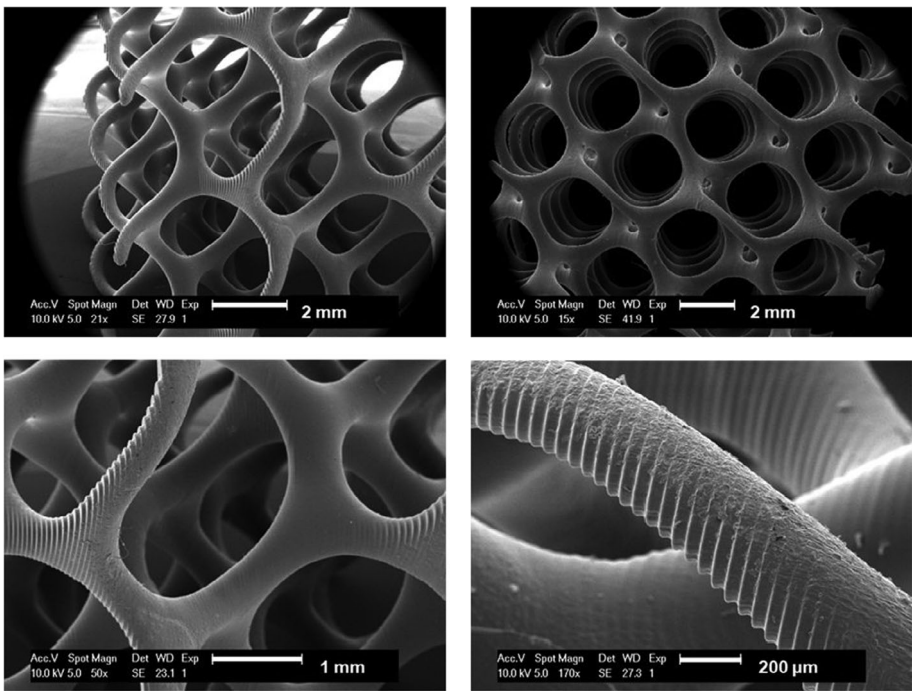

Figure 7. SEM imaging of the scaffold printed with DVS10 at varying magnifications.

sulfonate ester–acrylate systems the reaction rate of the photopolymerization is still fast enough, so that the printing time remains equal while a reduction of stress in the material could be achieved. At this point it has to be mentioned that thiol–acrylate systems of comparable thiol concentration are expected to show similar results, especially when considering the above discussed photorheology results and previous literature.[25,26]

Finally, the rest of the DVS10 formulation was used to print a chess figure and a scaffold to showcase two structures with more challenging geometries. After cleaning the printed parts with compressed air and isopropanol in an ultrasonic bath, the UV curing step serves to react residual acrylates in the material to receive a fully cured 3D-printed part with final mechanical properties. After post-processing the printed parts, the scaffold was investigated using SEM, which revealed smooth, highly resolved structures (Fig. 7). In the images with higher magnification, the layer-by-layer structure is clearly visible and matches the predetermined layer height of 50 μm.

CONCLUSIONS

We assessed the regulation of a difunctional acrylate matrix by means of CTAs. A state-of-the-art dithiol was compared to a difunctional vinyl sulfonate ester with similar linker. As expected, the thiol-containing formulations showed slightly retarded, yet fast photopolymerization with a high DBC. The difunctional vinyl sulfonate ester formulations exhibited a slightly slower curing behavior. The normal force measurements, which are used as a measure for the evaluation of shrinkage-induced stress in the photopolymerized specimens, revealed that both CTAs can reduce the shrinkage stress whereby the vinyl sulfonate ester-containing polymers led to lower normal force values compared to the thiol-regulated polymers.

Furthermore, DVS formulations exhibited superior storage stability and therefore address a critical issue in the use of thiols as CTAs.

Thermomechanical results demonstrated the efficient regulating performance of the CTA systems leading to more homogeneous network architectures, which are indicated by narrower and higher tan δ peaks in DMTA. In contrast to the thiol-regulated photopolymers, the DVS-regulated samples can maintain higher T_g and moduli at room temperature at equal concentrations. While softening due to reduced network density was evident particularly in nanoindentation experiments, the mechanical performance of DVS-containing polymers was significantly increased compared to both DT-containing polymers and the pure polyacrylate. Higher tensile strengths at similar elongations at break were evident and higher impact resistance was obtained. Finally, HDDA was 3D-printed with and without the addition of an optimal amount of DVS (10 mol%), which led to significantly improved printing results due to decreased shrinkage during curing.

ACKNOWLEDGEMENTS

The authors acknowledge TU Wien Bibliothek for financial support through its Open Access Funding Programme.

SUPPORTING INFORMATION

Supporting information may be found in the online version of this article.

REFERENCES

1 I. Campbell, O. Diegel, R. Huff, J. Kowen and T. Wohlers, *Wohlers Report 2020. Additive Manufacturing and 3D Printing: State of the Industry*, Wohlers Associates, Inc., Fort Collins, Colorado, USA; (2020).
2 Ligon-Auer SC, Schwentenwein M, Gorsche C, Stampfl J and Liska R, *Polym Chem* **7**:257–286 (2016).
3 Hoyle CE and Bowman CN, *Angew Chem Int Ed* **49**:1540–1573 (2010).
4 Carioscia JA, Lu H, Stanbury JW and Bowman CN, *Dent Mater* **21**: 1137–1143 (2005).
5 Wei H, Senyurt AF, Jönsson S and Hoyle CE, *J Polym Sci A Polym Chem* **45**:822–829 (2007).
6 Senyurt AF, Wei H, Hoyle CE, Piland SG and Gould TE, *Macromolecules* **40**:4901–4909 (2007).
7 Podgórski M, Becka E, Claudino M, Flores A, Shah PK, Stansbury JW *et al.*, *Dent Mater* **31**:1255–1262 (2015).
8 Esfandiari P, Ligon SC, Lagref JJ, Frantz R, Cherkaoui Z and Liska R, *J Polym Sci A Polym Chem* **51**:4261–4266 (2013).
9 Podgórski M, Wang C, Yuan Y, Konetski D, Smalyukh I and Bowman CN, *Chem Mater* **28**:5102–5109 (2016).
10 Moad G, Rizzardo E and Thang SH, *Polymer* **49**:1079–1131 (2008).
11 Yagci Y and Reetz I, *React Funct Polym* **42**:255–264 (1999).
12 C. T. Berge and V. Desobry, Molecular weight controlled polymers by photopolymerization. WO Patent 9837104 (1998).
13 Kloxin CJ, Scott TF and Bowman CN, *Macromolecules* **42**:2551–2556 (2009).
14 Okamura H, Yamagaki M and Nakata K, *Polymers* **11**:5 (2019).
15 Peer G, Eibel A, Gorsche C, Catel Y, Gescheidt G, Moszner N *et al.*, *Macromolecules* **52**:2691–2700 (2019).
16 Shah PK, Stansbury JW and Bowman CN, *Polym Chem* **8**:4339–4351 (2017).
17 Gorsche C, Griesser M, Gescheidt G, Moszner N and Liska R, *Macromolecules* **47**:7327–7336 (2014).
18 Gorsche C, Koch T, Moszner N and Liska R, *Polym Chem* **6**:2038–2047 (2015).
19 Gauss P, Ligon-Auer SC, Griesser M, Gorsche C, Svajdlenkova H, Koch T *et al.*, *J Polym Sci A Polym Chem* **54**:1417–1427 (2016).
20 Gorsche C, Seidler K, Harikrishna R, Kury M, Koch T, Moszner N *et al.*, *Polymer* **158**:149–157 (2018).
21 Ganster B, Fischer UK, Moszner N and Liska R, *Macromolecules* **41**: 2394–2400 (2008).
22 Gorsche C, Harikrishna R, Baudis S, Knaack P, Husar B, Laeuger J *et al.*, *Anal Chem* **89**:4958–4968 (2017).
23 Nouailhas H, Aouf C, Le Guerneve C, Caillol S, Boutevin B and Fulcrand H, *J Polym Sci A Polym Chem* **49**:2261–2270 (2011).
24 Zhao S and Abu-Omar MM, *ACS Sustain Chem Eng* **4**:6082–6089 (2016).
25 Shaukat U, Rossegger E and Schlögl S, *Polymer* **231**:124110 (2021).
26 Ahn D, Stevens LM, Zhou K and Page ZA, *Adv Mater* **33**:2104906 (2021).

